Comparisons of Multilayer H_2O Adsorption onto the (110) Surfaces of α-TiO_2 and SnO_2 as Calculated with Density Functional Theory

Andrei V. Bandura,[†] James D. Kubicki,[*,‡] and Jorge O. Sofo[§]

Department of Quantum Chemistry, The St. Petersburg State University, St. Petersburg, Russia, and Department of Geosciences and the Earth & Environmental Systems Institute, and Department of Physics, The Pennsylvania State University, University Park, Pennsylvania 16802

Received: December 14, 2007; Revised Manuscript Received: June 14, 2008

Mono- and bilayer adsorption of H_2O molecules on TiO_2 and SnO_2 (110) surfaces has been investigated using static planewave density functional theory (PW DFT) simulations. Potential energies and structures were calculated for the associative, mixed, and dissociative adsorption states. The DOS of the bare and hydrated surfaces has been used for the analysis of the difference between the H_2O interaction with TiO_2 and SnO_2 surfaces. The important role of the bridging oxygen in the H_2O dissociation process is discussed. The influence of the second layer of H_2O molecules on relaxation of the surface atoms was estimated.

1. Introduction

Crystalline surface structure has a strong influence on the surface chemistry of metal oxides and water structure in the interfacial region. The ionic nature of the most metal oxides leads to a predominance of acid−base interactions where metal cations and oxygen anions are acidic and basic sites, respectively, and their reactivity is described in terms of the acid/base properties of particular sites in relation to their bonding environment. Thus, the 3-D arrangement of atoms on bare and hydrated surfaces of oxides is one of the key factors in controlling the surface reactivity. Understanding how surface structure influences the surface chemistry of metal oxides is of importance for catalysis, ceramic materials synthesis, and environmental science.

α-TiO_2 (rutile) and SnO_2 (cassiterite) are widely used in the different areas of technology and industry. Both of these minerals have the rutile structure, and the (110) surface is the most stable when the materials are stoichiometric. Although they have similar structures, SnO_2 and TiO_2 are electronically different because Ti is a transition element and Sn is a group IV element.

Two types of adsorption are possible on a (110) surface: (1) molecular, with formation of a bond between the H_2O O atom and 5-fold coordinated atom of the metal; and (2) ionic or dissociative, when one of the H_2O protons transfers to the bridging O atom. Mixed states between these two end-members are common.

The rutile α-TiO_2 (110) surface is one of the most extensively studied oxide surfaces in the literature using experimental[1−3] and theoretical[4−10] methods and is one of the most controversial cases with regards to molecular versus dissociative adsorption. Goniakowski and Gillan[4] published one of the earliest papers on first-principles calculations of H_2O adsorption on the TiO_2 (110) surface. In this paper, the first comparison of water adsorption on TiO_2 and SnO_2 (110) surfaces was made using density functional theory (DFT) methods. Later the quantum mechanical studies of H_2O adsorption on TiO_2 have been conducted by Lindan et al.,[5,6] Bates et al.,[7] Langel,[8] Bandura et al.,[9] and Perron at al.[10] Most calculations were carried out at the DFT level using the pure functionals in generalized gradient approximations (GGA) and planewave (PW) basis,[4−8,10] whereas a few calculations were reported using the Hartree−Fock (HF) approximation and the linear combination of atomic orbitals (LCAO).[9] While, as it was determined in recent works,[5−10] the molecular sorption of water is energetically favorable in a monolayer on a (110) rutile surface, the dissociative type of adsorption can also be envisaged because it could be stabilized with hydrogen bonding. Thus, using a large 2×3 surface supercell with different ratios of molecular/dissociated water molecules, Perron et al.[10] in their most recent PW GGA study found that with up to 33% of dissociated water molecules, the destabilization due to water dissociation is greatly compensated by hydrogen bonds. This result is consistent with experimental data[3] suggesting that 10−25% of the first hydration layer could be dissociated.

Further comparison of water adsorption on TiO_2 and SnO_2 (110) surfaces was made[11,12] using the PW GGA calculations and in ref 13 using the hybrid B3LYP[14,15] exchange-correlation functionals and LCAO basis set. Water dissociation on SnO_2 surfaces was calculated to be more favorable than on the similar TiO_2 surfaces. Moreover, at low coverages the molecular form of H_2O seems to be unstable on the (110) SnO_2 surface.

The objective of this paper is to analyze factors that explain the differences between the H_2O adsorption on rutile and cassiterite (110) surfaces at different coverages. The main motivating factor for this comparison is the conclusion of Sverjensky[16] that the bulk dielectric constant of the solid influences the structure of water at the oxide−water interface and subsequently controls adsorption.

2. Computational Details

All calculations were performed using the planewave pseudopotential implementation of density functional theory (DFT) as written into the VASP code.[17,18] Exchange and correlation were treated within the Perdew−Burke−Ernzerhof (PBE) functional.[19] The PBE functional is frequently used now for DFT calculation of solids and their surfaces. Our experience shows

* Corresponding author. E-mail: kubicki@geosc.psu.edu.
† The St. Petersburg State University.
‡ Department of Geosciences and the Earth & Environmental Systems Institute, The Pennsylvania State University.
§ Department of Physics, The Pennsylvania State University.

10.1021/jp711763y CCC: $40.75
Published on Web 08/20/2008

TABLE 1: Results of the Bulk Unit Cell Optimization

crystal	*a*, Å	*c*, Å	*u*	reference
TiO_2	4.653	2.972	0.3049	this work
	4.594	2.959	0.305	experiment[27]
SnO_2	4.828	3.245	0.3065	this work
	4.737	3.186	0.306	experiment[28]

that, concerning the formation energy and geometry of bulk and surface systems, PBE GGA frequently produces the results which are very close to PW91 GGA of Perdew and Wang.[20] However, unlike PW91 it has unempirical derivations[19] based on exact properties of the exchange-correlation energy. For this reason, PBE functional best fulfills many of the physical and mathematical requirements of DFT.

Ionic cores were described by the projector-augmented wave (PAW) method[21,22] which improves transferability and reduces the number of planewaves required in the expansion of the Kohn−Sham orbitals in order to improve computational efficiency. For Ti, a pseudopotential in which the semicore states (3s and 3p) were treated as valence electrons was used. Similarly, the valence shell of Sn included the 4d-states. Medium-range values of the energy cutoff, 400 eV, have been applied in all calculations. Γ-centered Monkhorst−Pack[23] 4 × 4 × 6 grid was used for the Brillouin zone sampling in bulk crystal calculations. An extended grid (16 × 16 × 24) was applied to generate the electronic density of states (DOS). For surface calculations, the number of *k*-points was decreased proportionally corresponding to the reduction of the Brillouin zone. The convergence criterion in the electronic cycle (i.e., computation of the electron probability density) was set to 10^{-6} for bulk and bare surface slabs, whereas for H_2O-containing systems, 10^{-4} was used. Using the same pseudopotentials, energy cut-offs and other simulation parameters are essential for correct comparison of the two minerals.

To provide a more precise estimation of atomic relaxations and surface and adsorption energies, the lattice constants a and *c* of the tetragonal bulk unit cell were optimized. To this purpose, the set of constant-volume calculations were made, and the resulting energies were fit to analytical expression. The obtained lattice parameters are given in Table 1. Calculated values for rutile are accurate to 1% and for cassiterite to 2%.

Surfaces were modeled using slab geometries of periodically repeated 2 × 1 supercells containing up to five Me layers (15 atomic planes). A layer is thus defined as consisting of three atomic planes, a Me_2O_2 plane and the atomic O planes above and below it, that together form a stoichiometric entity. Five Me_2O_2 layers are sufficient[24−26] for reproducing the topmost atoms relaxation and for correct estimation of the H_2O adsorption energies. A vacuum width of 14 Å separated the slab from its periodic image and proved to be sufficient to avoid interactions between the adsorbed (up to third layer) H_2O molecules on repeated slabs. With the five-Me-layer-thick slab this led to 30 Å third translation vector. The energy of an isolated H_2O molecule was calculated using the periodic cell of 10 Å. Inversion symmetry (space group $P\bar{1}$) was imposed on all systems containing H_2O molecules to ensure the equivalence of the both slab sides. The relaxation of all atomic positions in slabs was allowed except for the atoms in the middle layers of the TiO_2 and SnO_2 slabs. This approach allows a thin slab to better mimic the behavior of the surface of a bulk solid (Bandura and Kubicki, 2003). Energy minimizations were carried out until all forces on atoms were less than 0.01 eV/Å for bare surface slabs, and less than 0.05 eV/Å for hydrated slabs. (Note: the less stringent relaxation condition for hydrated slabs is due to the fact that small variations in H-bonding configurations cause potential energy changes of this magnitude, making the smaller convergence criterion impractical.)

To simulate adsorption of two layers of water, eight H_2O molecules were placed on each side of the surface slab unit cell. The same five-Me-layer 2 × 1 supercell was used as in study of the monolayer adsorption. To prepare reasonable initial structures, a previously derived force field[29] was used in classical molecular dynamics (CMD) simulation of the SnO_2-H_2O system. For each type of coverage, we have generated a long (∼100 ps) CMD trajectory. Several low energy intermediate states were picked from each trajectory as probable initial structures. After static optimization with the force field, the most low-energy state was chosen for further quantum mechanical investigations. The system generated in this manner was used for creating the corresponding TiO_2-H_2O system by scaling the atomic coordinates to TiO_2 cell dimensions. Hence, the initial configurations for both systems were similar and should not contribute to the differences seen in the final configurations.

3. Results and Discussion

3.1. Relaxation of Bare Surfaces. Relaxation of the bare surfaces was calculated first. These calculations provide the energies needed for calculations of the H_2O adsorption energies. In addition, these calculations allow estimation of the surface energies. Obtained surface energies are given in Table 2. In this table, we also compare the vertical displacements of the surface atoms relative to their bulk positions that have been

TABLE 2: Comparison of the Calculated Surface Energy and Vertical Relaxation of the Top Surface Atoms[a] for the Bare (110) Surfaces of TiO_2 and SnO_2 (results for five-Me-layer slabs)

crystal	surface energy, J m^{-2}	*z*-shifts, Å					bond length $Me_{VI}-O_{br}$, Å	reference method
		Me_{VI}	Me_V	O_{br}	O_{surf}	O_{subbr}		
TiO_2	0.53	0.20	−0.16	0.00	0.17	−0.01	1.83−1.85[b]	this work
	0.55	0.31	−0.13	0.09	0.22	0.08	1.85[31]	LCAO PBE0[30]
	0.81	0.09	−0.12	−0.09	0.11	−0.05		PW PW91[24]
	0.90	0.26	−0.15	0.06	0.17	−		PW LDA[25]
		0.25	−11	0.10	0.17	0.17		experiment[2]
		±0.01	±0.01	±0.04	±0.03	±0.04		
SnO_2	1.03	0.20	−0.10	0.06	0.18	0.04	2.01[b]	this work
	1.28[c]	0.21	−0.12	0.05	0.14	0.04	1.93[d]	LCAO B3LYP[13]
	1.04	0.22	−0.11	0.09	0.18	0.07		PW PW91[26]

[a] Me_{VI}, 6-fold coordinated surface Me; Me_V, 5-fold coordinated surface Me; O_{br}, bridging oxygen; O_{subbr}, oxygen underneath O_{br}; O_{surf}, 3-fold coordinated surface oxygen. [b] Me−O bond length is 1.96 Å in bulk TiO_2 and 2.09 Å in bulk SnO_2 optimized cells. [c] LCAO B3LYP result[13] corrected for the basis set superposition error (BSSE). [d] LCAO B3LYP results;[13] Sn−O bond length is 2.03 Å in bulk SnO_2 optimized cell.

TABLE 3: H_2O Adsorption Energies (i.e., energy required to desorb 1 mol of H_2O) for (110) Surfaces of TiO_2 and SnO_2

			adsorption energy per H_2O molecule, kJ/mol			
crystal	number of Me_2O_4 layers	one side of 2 × 1 surface cell	assoc adsorp	mixed adsorp	dissoc adsorp	reference
TiO_2	3	2	92		83	unpublished[a]
	5	2	83	81	66	this work
			96	97	88	5
	5	8	61	60	58	this work
SnO_2	3	2		143	146	29
	5	2	(113)[b]	143	141	this work
			125		159	13 [c]
				171	166	11
	3	8		79	79	this work
	5	8		78	79	this work

[a] Results of our calculation using E_{cutoff} = 700 eV. [b] Unstable structure, obtained with constrains for the H_2O oxygen movement. [c] LCAO B3LYP result.[13] (BSSE-corrected values).

calculated from the equilibrium slab geometry. The data in Table 2 show that our results for vertical shifts agree well with both experimental and theoretical available data. More importantly, debate over the relaxation of the surface-bridging oxygen has been resolved in the recent surface X-ray diffraction measurements.[2]

Our previous experience show that the final atomic relaxations may depend (to some extent) on the structure adopted as initial for optimization. Particularly, the high initial symmetry does not break spontaneously and tends to be retained in the final structure. That is why, in contrast to the other studies, we have investigated the role of a symmetry break by allowing lateral relaxation as well as vertical. For this purpose, the bridging O atoms in the primitive (1 × 1) surface unit cell were shifted by 0.15 Å in the (001) direction from their symmetrical positions before the optimization. Additionally, the relaxation of the extended 2 × 1 surface unit cell was studied. To catch the possible symmetry-breaking, we removed the water hydrogens and oxygens from the optimized hydroxylated 2 × 1 slabs (for monolayer coverage) and took them as the initial structures for the bare surface slabs. In this case the all-surface atoms have some initial lateral shifts in both (001) and ($\bar{1}$10) directions.

All regarded slab systems (using and 1 × 1 and 2 × 1 surface unit cells) produced practically equal results for atomic distortions and surface energy. In the final structures, only the TiO_2 slab exhibited a slight deviation from the *Pmmm* symmetry: the two Ti(VI)—O_{br} distances differ by about 0.01 Å. Also, 3-fold O_{surf} atoms have the well-distinguishable lateral shifts (0.05—0.06 Å) in ($\bar{1}$10) and (1$\bar{1}$0) directions toward the 5-fold Ti or Sn atoms. The latter fact agrees well with the results of ref 30.

There is a noticeable difference for the calculated TiO_2 surface energies. The values reported earlier in the literature[24,25] are larger than ours. However, our data are in excellent agreement with the recent results of Perron et al.[31] obtained using the PAW pseudopotentials and PW91 functionals in PW DFT calculations of TiO_2 surface systems. The same conclusion becomes true when we compare our data with results of the latest LCAO investigation of Labat et al.,[30] where the Hartree—Fock, plain and hybrid DFT-LCAO techniques (B3LYP[14,15] and PBE0[32]) were applied for study of TiO_2 surface relaxation. The larger surface energies for the rutile (110) surface obtained in early studies might be a result of neglecting lateral relaxation of surface atoms and assuming that only vertical relaxation occurred. Nevertheless, relatively small lateral shifts obtained in our and other[30] calculations give evidence that contribution of lateral relaxations cannot be large. So, the difference between calculated surface energies may be primarily due to inequality of DFT Hamiltonians and pseudopotentials used in previous works[24,25] and in our and the recent studies.[30,31] Also, there is a possibility, that more careful choice of unit cell parameters reduced the errors for estimated surface energies. On the basis of our and the other most recent results[30,31] we can suggest that 0.5 J/m^2 is a reliable value for the surface energy of (110) TiO_2 surface.

Taking into account the results in Table 2, we conclude that the surface energy of SnO_2 (110) surface is noticeably larger (about 1.0 J/m^2) than the surface energy of TiO_2 crystal (about 0.50 J/m^2) even though the relaxation of the surface atoms is similar for both crystal surfaces except for the 5-fold metal atom which has a slightly large inward displacement in the case of TiO_2.

3.2. DOS for Bare and Hydrated Surfaces. Previous DFT calculations[11,12] have predicted significant differences in the structure of adsorbed H_2O on (110) TiO_2 (rutile) and SnO_2 surfaces where the dissociative adsorption was favored on SnO_2 versus associative adsorption on TiO_2. Lindan[11] attributed the difference in H_2O behavior on the surface to the larger 2-D

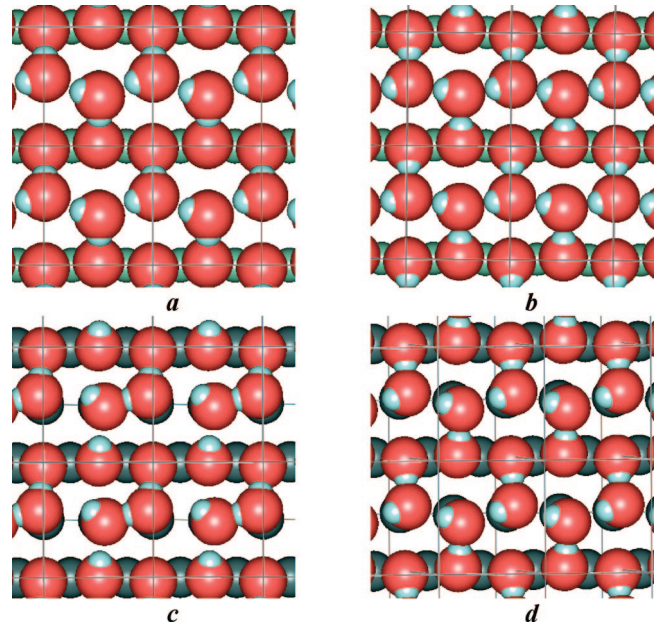

Figure 1. The similarity of the first adsorption layer in rutile and cassiterite. View in the (110) direction: (a) associative adsorption on TiO_2; (b) dissociative adsorption on TiO_2; (c) mixed adsorption on SnO_2; (d) dissociative adsorption on SnO_2. Oxygen atoms: red; metallic atoms: gray; hydrogen atoms: light-blue. (Graphical representation of molecular models has been made with WebLab ViewerLight program, v 3.7).

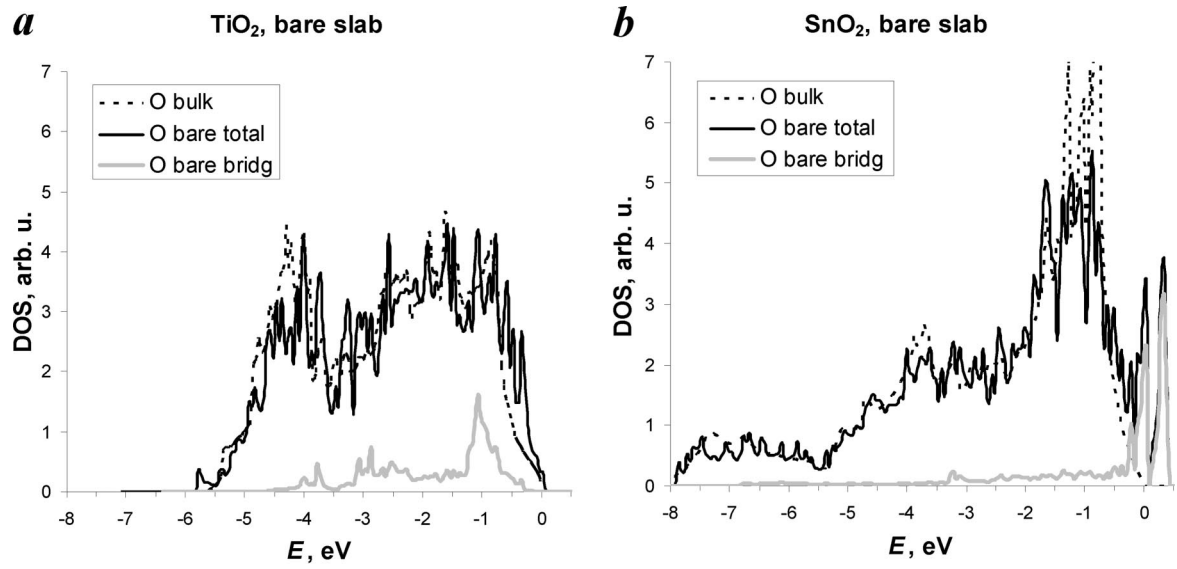

Figure 2. Change of oxygen contribution to VB DOS during the surface formation in TiO_2 (a) and SnO_2 (b) crystals. Dotted lines represent the total O contribution to the bulk DOS, and solid lines represent the total O contribution to the five-layer slab DOS. The contribution of bridging oxygens (given in bold gray) forms a sub-band at the top of SnO_2 VB, indicating the strong basicity of O_{br} in this crystal.

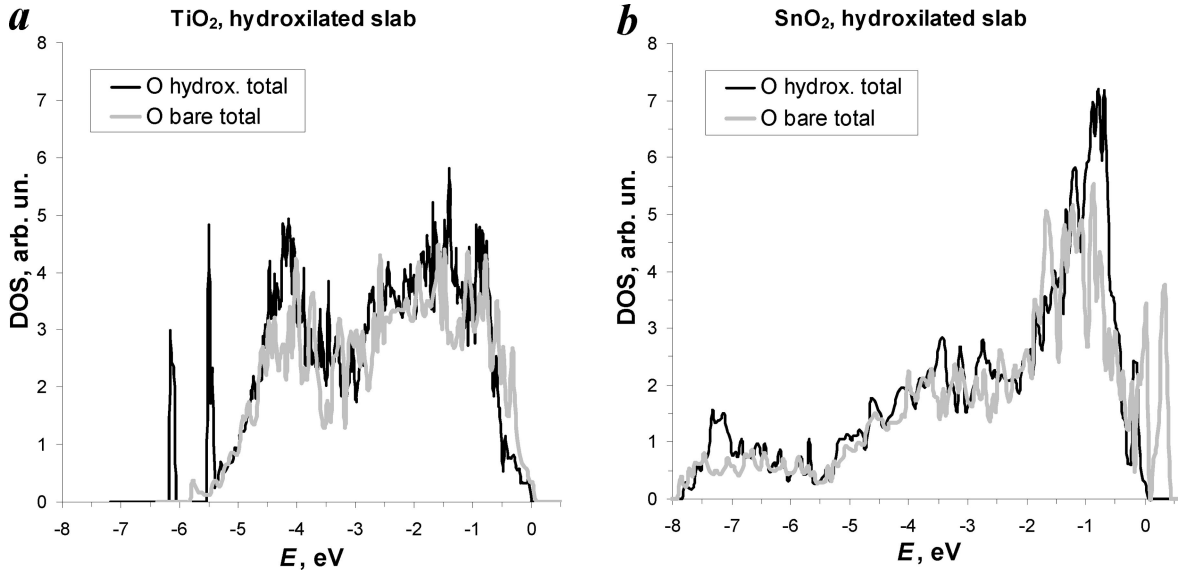

Figure 3. Change of total O contribution to VB DOS during the hydroxylation (mixed case) of the surface in TiO_2 (a) and SnO_2 (b) crystals. The comparison of oxygen contribution for hydroxylated slabs (solid curves) and oxygen contribution for bare slabs (thick gray curves) shows the different nature of changes upon hydroxylation for the two surfaces.

unit cell parameters of SnO_2 compared to those of TiO_2 (experiment values: $a = 3.186$, $b = 6.699$ Å; vs $a = 2.959$, $b = 6.497$ Å, respectively). The larger unit-cell dimensions caused H-bonding among the adsorbed H_2O molecules on the surface to be less energetically important on SnO_2 than TiO_2. This can be seen in our results as well (Figure 1) where the plan view of the hydrated surfaces are given. In the case of TiO_2, similar 2-D H-bond networks are formed both for associatively and dissociatively hydrated surfaces, whereas in the case of the SnO_2, dissociation is needed for formation of the 2-D H-bond network.

Calatayud at al.[33] pointed out that molecular adsorption on an oxide surface can be understood as an acid−base process. From this point of view, the more covalent character of the Sn−O bonds compared to the corresponding Ti−O bonds might be another factor that causes the dissociation of H_2O on the SnO_2 surface.[11,13] In fact, the electronegativity of Sn (1.8) is remarkably greater than electronegativity of Ti (1.4). The significant reduction of the top surface Sn(V) charges[13] correlates with the higher electronegativity of Sn. As a result, the hydrated Sn(V) ion perhaps is a stronger Brønsted acid than the hydrated Ti(V) ion on the rutile surfaces. Water hydrolysis can be promoted further by the larger basicity of the bridging oxygens (see discussion below).

In the initial stage of our calculations, two H_2O molecules were placed on each side of the slab supercell to simulate the full-monolayer coverage. In the case of the TiO_2 (110) surface, stable molecular adsorption was obtained after energy minimization. In the case of SnO_2 (110) surface, one of the two H_2O molecules on each face dissociated thus producing a mixed molecular-dissociative structure. A similar mixed structure for the TiO_2 surface was created by transferring a H^+ from one of the H_2O molecules in the previously obtained molecular structure along the O−H···O H-bond to the nearest bridging oxygen. Starting with the dissociated H_2O molecules, we also obtained stable dissociated structures on both surfaces where hydroxyls were attached to 5-fold coordinated metal atoms, and

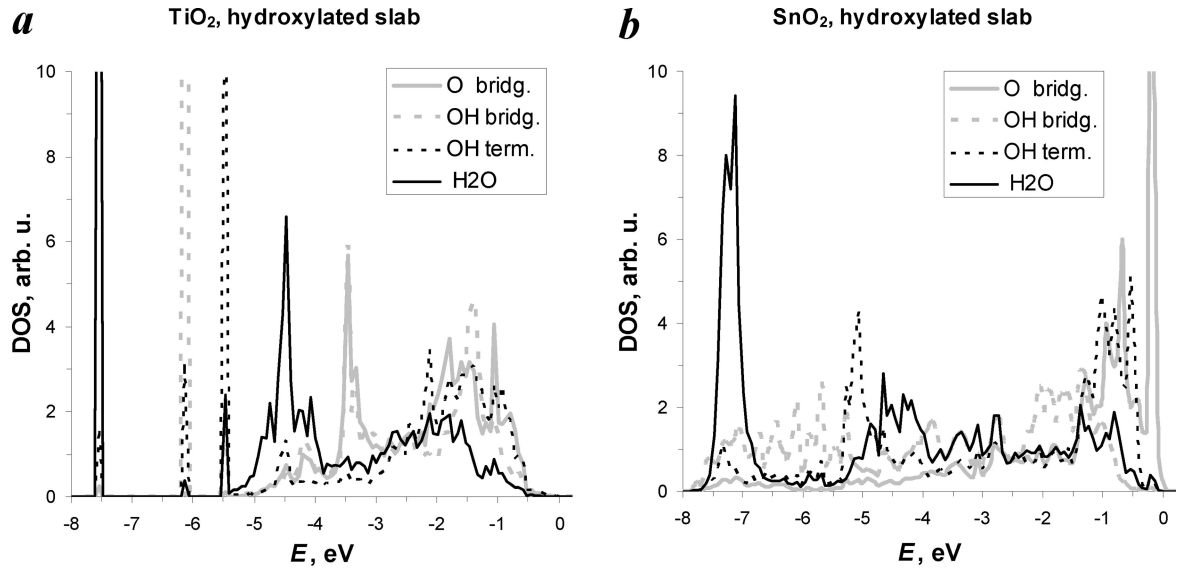

Figure 4. Surface-group contributions to the VB DOS for the hydroxylated (mixed case) surfaces in TiO_2 (a) and SnO_2 (b) crystals. The comparison of group contributions (H_2O, solid curves; OH terminal group, black dotted curves; OH bridging group, gray dotted; unprotonated bridging O, thick gray curves) shows the different position of their main peaks relative the VB of two regarded crystals.

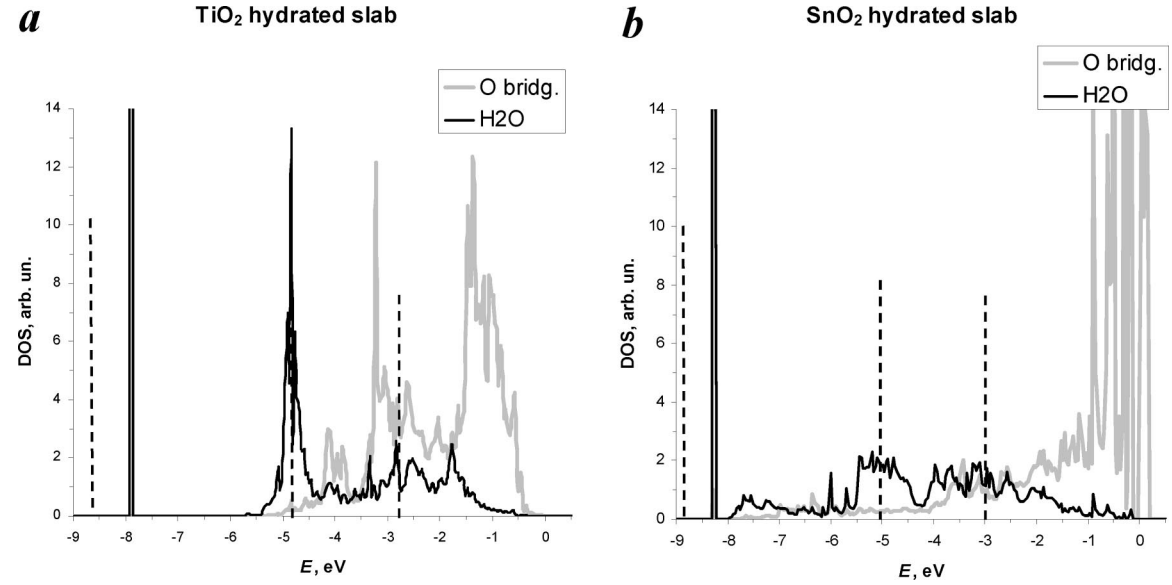

Figure 5. Contributions of bridging oxygens (thick gray lines) and water atoms (solid lines) to the VB DOS for the hydrated (at half-monolayer coverage) surfaces in TiO_2 (a) and SnO_2 (b) crystals. The broader and lower H_2O peaks in SnO_2 demonstrate the strong water−surface interaction. The positions of electronic levels in isolated H_2O molecule are given by the vertical dash lines.

H^+ were bonded to the bridging oxygens. Plan views of the optimized structures are given in Figure 1, where the similarity of the all hydrated surfaces is clarified. Resulting adsorption energies (Table 3) agree well with results of the available theoretical calculations.[5,11,13,29] Optimized structures for the mixed type of H_2O adsorption were used for the DOS analysis.

Oxygen p-states are the main contributors to valence-band (VB) DOS of most metal oxides.[33] Goniakowski and Gillan[4] were the first who noticed the difference between the distribution of the electronic states in TiO_2 and SnO_2 surfaces. We performed similar calculations except that we used five-Me-layer slabs rather than three-Me-layer slabs. We compare the obtained total and projected DOS of the valence band for bulk and (110) surfaces of TiO_2 and SnO_2 in Figure 2. The zero energy is taken at the Fermi level of the bulk crystal, and all curves were shifted in such a way that most of the peaks in the central part of VB coincide. All DOS values have been calculated per one Me_2O_4 formula unit in the solid phase to permit comparison on an equal scale.

Figure 2 shows that a new O_{br}-sub-band appears in the surface systems at the top of the bulk VB in the case of SnO_2 only. The contribution of the bridging oxygens on the TiO_2 surface lays entirely in the VB. This fact indicates that basicity of O_{br} in SnO_2 should be larger than the basicity of O_{br} in TiO_2 because the electronic energy levels are significantly higher than the bulk.[33]

The important role of the bridging oxygen in the dissociation process[33] is confirmed by the comparison of their contribution to valence-band DOS for bare and hydroxylated (110) surface slabs (Figures 3 and 4). Figures 3b and 4b illustrate that protonation of one bridging oxygen on the (110) SnO_2 surface leads to reduction and shifting of the unprotonated O_{br} peaks toward the bulk valence band states. This means that protonation

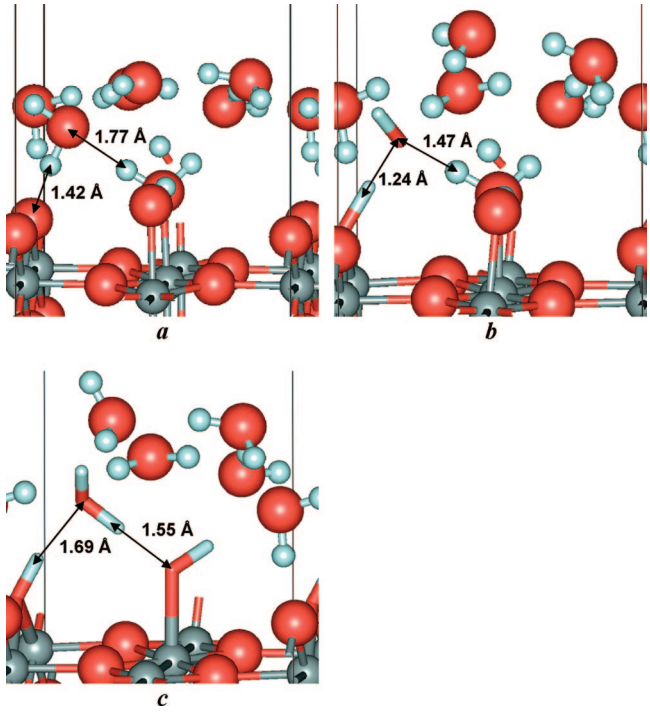

Figure 6. Initial (a), intermediate (b), and final (c) structures in the optimization pathway for eight H_2O molecules adsorbed on (110) SnO_2 surface. These subsequent structures illustrate the indirect path for the spontaneous proton transfer when the direct H^+ transfer from water to bridging oxygen is obstructed. Hydroxyl groups, intermediate ion OH^-, and the resulting H_2O molecule are displayed in stick mode. See Figure 1 for the atom color code.

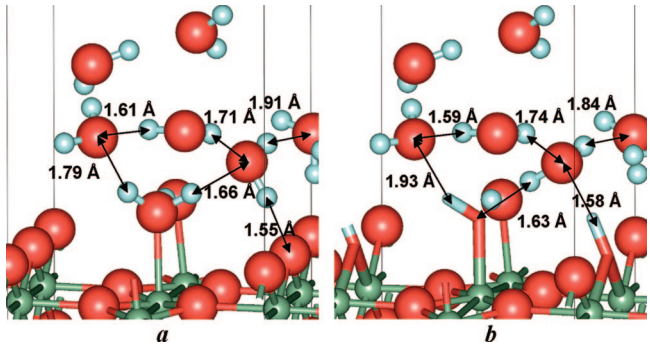

Figure 7. DFT-optimized structures for the adsorption of 8 H_2O molecules on (110) TiO_2 surface (terminal and bridging OH-groups are shown as sticks): molecular (a) and mixed adsorption (b). Second-layer molecules above the L1 water cannot form H-bonds with surface groups. See Figure 1 for the atom color code.

of one bridging oxygen on the SnO_2 surface through dissociation[33] leads to reduction of the basicity of the adjoining bare bridging oxygen, and as a consequence, spontaneous dissociation of the second H_2O molecule does not occur. Similar nonlocal effects have been calculated for PbS by Rosso and Becker.[34]

No such effect was found for the bridging oxygen on the (110) TiO_2 surface (Figures 3a and 4a). Only a reduction in the height of the corresponding peak relative to the bare surface case occurs and no considerable shift toward the VB states was predicted. Moreover, the DOS distributions in the high energy regions for protonated and unprotonated bridging oxygens are similar.

The electrons of the protonated O atoms and H_2O on the hydrated TiO_2 surface form localized states at energies <5 eV, just below the bottom of VB (Figure 4a). In the case of the

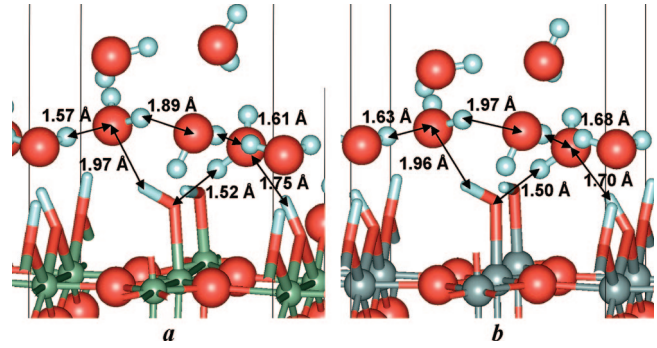

Figure 8. Optimized structure for dissociative adsorption of eight H_2O molecules on (110) TiO_2 (a) and SnO_2 (b) surface (terminal and bridging OH groups are shown as sticks). Second-layer molecules can form short H-bonds with both the terminal and bridging hydroxyl groups. See Figure 1 for the atom color code.

hydrated (110) SnO_2 surface, such states proved to be completely within the VB of the crystal and do not exhibit sharp localized futures except the H_2O peak between -8 and -7 eV. However, this peak is noticeably wider than the corresponding peak in the hydrated TiO_2 DOS.

To investigate the reorganization of electronic states after adsorption of H_2O molecules, we calculated the associative adsorption of one H_2O molecule on a 2×1 cell surface. Corresponding initial structures have been prepared by removing the dissociated H_2O from the mixed-adsorption structures. In these systems, the H_2O molecules were separated from each other by 6 Å or more, so there is no strong H_2O-H_2O interaction. The molecular form of a single H_2O is unstable in the case of SnO_2 (110) surface. To prevent the spontaneous dissociation of H_2O, O movement was restricted in the direction $1\bar{1}0$ during the optimization of the H_2O-SnO_2 system.

The contributions of H_2O and bridging oxygen atoms to the total DOS in optimized half-monolayer structures are shown in Figure 5. Included in Figure 5 is the DOS for the isolated H_2O molecule. The distribution for the isolated H_2O has been shifted such that the position of its middle peak coincided with the position of the middle peak for the adsorbed H_2O. Only the lowest H_2O peak (near -8 eV) preserves its highly localized nature for the both surfaces (Figure 5). The second H_2O peak also is very sharp in the case of the TiO_2 surface, whereas it disappears in the case of SnO_2 surface. On the basis of these observations, we conclude that redistributions of electronic states is stronger for H_2O adsorption on the (110) SnO_2 surface compared with the corresponding TiO_2 surface.

3.3. Multilayer Adsorption. Up to eight H_2O molecules on each side of the surface slabs were considered. This amount is sufficient to form the first (L1) and the second (L2) adsorption layers on the surface.[35] As found earlier,[5,6,9] the increasing number of H_2O molecules on the surface stabilized associative adsorption. Hence, it might be expected that for both crystals we could obtain stable molecular coverage. However, starting with the associated H_2O molecules, we have obtained the mixed associative−dissociative structure in the case of SnO_2. (Figure 6c).

The most interesting phenomenon observed is that dissociation of H_2O occurred indirectly in the investigated structure. In the first stage, the H^+ transferred to bridging oxygen from one of the nearest H_2O molecules above O_{br}, forming the intermediate OH^- state. In the second stage, a H^+ from the terminal H_2O transfers to an OH^- ion forming a new H_2O molecule and terminal hydroxyl connected by a short (1.55 Å) H-bond. This suggests that the first adsorption layer (L1) on SnO_2 (110)

TABLE 4: Relaxations of Top Metal Ions and Heights of O Atoms of Adsorbed H_2O Molecules Relative the Bulk Position of Top Me-Layer on the (110) Surfaces of TiO_2 and SnO_2 (averaged results for five-Me-layer slabs and for $N_w = 2$ and $N_w = 8$ H_2O molecules on each side)

		z-shifts or O positions, Å					
		assoc adsorption		mix. adsorption		dissoc adsorption	
crystal	atom[a]	$N_w = 2$	$N_w = 8$	$N_w = 2$	$N_w = 8$	$N_w = 2$	$N_w = 8$
TiO_2	Ti_{VI}	+0.13	+0.09	+0.04	+0.02	−0.03	−0.03
	Ti_{term}			+0.10	+0.10	+0.10	+0.09
	Ti_V	−0.12	−0.09	−0.11	−0.10		
	O_{br}	0.00	−0.03	−0.03	0.00		
	$O_{br(H)}$			+0.06	−0.03	+0.05	+0.03
	O_{surf} [b]	+0.08	+0.07	+0.05	+0.04	+0.03	+0.02
	O_{term}			2.02	2.07	1.98	2.01
	O_{H2O}	2.17	2.15	2.09	2.08		
SnO_2	Sn_{VI}	(+0.10)[c]		+0.02	+0.03	−0.04 (−0.05)	−0.04
	Sn_{term}			+0.01	+0.03	+0.03 (+0.04)	+0.03
	Sn_V	(−0.06)		−0.04	−0.02		
	O_{br}	(+0.05)		−0.01	0.00		
	$O_{br(H)}$			+0.07	+0.04	+0.04	+0.03−0.01
		+0.03	+0.03	+0.03	+0.03	+0.03	+0.03(+0.02)
	O_{surf}[a]	(+0.05)		+0.01	+0.03	−0.03 (−0.02)	−0.01
	O_{term}			2.05	2.11	2.03 (1.99)	2.08
	O_{H2O}	(2.06)		2.07	2.13		

[a] Ti_{VI} and Sn_{VI}, 6-fold coordinated surface Me; Ti_V and Sn_V, 5-fold coordinated surface Me; Ti_{term} and Sn_{term}, 6-fold coordinated terminal Me with OH group; O_{br}, unprotonated bridging oxygen; $O_{br(H)}$, protonated bridging oxygen; O_{surf}, 3-fold coordinated surface oxygen; O_{term}, terminal oxygen in OH group; O_{H2O}, water oxygen atom. [b] Actual (before averaging) displacements of O atoms in the top Me_2O_2 layer are large and may run up to ±0.1 Å and ±0.2 Å for the TiO_2 and SnO_2 surfaces, correspondingly. [c] LCAO B3LYP results[13] are given in parentheses.

surface cannot totally consist of undissociated water molecules even for the multilayer adsorption.

No such process was observed for the TiO_2 (110) surface, and a stable molecular structure (Figure 7a) was obtained by energy optimization. A stable mixed adsorption structure (Figure 7b) was obtained by optimization after manual H^+ transfer on the same path as was spontaneously passed in the case of SnO_2. Analogously, starting with the broken H_2O molecules in the first layer, we have obtained the stable dissociated structures both for TiO_2 and SnO_2 where hydroxyls were attached to 5-fold Me, and H^+ were bonded to the bridging oxygens (Figures 7a and 7b).

As discussed in Mamontov et al.,[35] in the presence of bulk water, the (110) surfaces of both rutile and cassiterite crystals exhibit three distinct surface layers (L1, L2, and L3) that have different characteristics relative to bulk water. The first sorbed layer, L1, involves exactly two protons (one water molecule or two hydroxyl groups) per Me_2O_4 surface unit. L2 water molecules exhibit specific axial and lateral (surface-parallel) site distribution densities that are influenced both by the underlying crystal structure and strong H-bonding with L1 and L3 species. Molecules in the third layer L3 do not have direct H-bonds to the L1 oxygen or H atoms, but their ordering and dynamics differ considerably from bulk. We do not have the completed L3 layer in our models with eight H_2O molecules, but the L1 and L2 layers are represented. From our results, it is clearly seen that the structure of the L1 predetermines the structure of L2. In particular, in the case of dissociative adsorption of L1, the L2 H_2O molecules can form strong H-bonds (exhibiting H—O distances of ≈1.5 Å) both with the bridging and terminal O atoms. In the case of a molecular form of L1, H_2O in L2 can primary interact via its H^+ with the bridging O atoms only. Thus, the nature of L1 (predominantly associative for TiO_2 and dissociative for SnO_2) leads to the difference between the hydration water dynamics in rutile and cassiterite.[35]

Energies calculated for adsorption of eight H_2O molecules are given in Table 3 together with the energies of monolayer adsorption which was calculated for the purpose of comparison. All quantities are given per one H_2O molecule. Comparisons of data in Table 3 show that H_2O adsorption on the (110) surface of TiO_2 is less energetically favorable than adsorption on SnO_2 surface. For the monolayer, the difference is about 50 kJ/mol, with H_2O preferring to be in molecular form on TiO_2 and in mixed form on the SnO_2 surface. Obtained monolayer adsorption energies for the (110) surfaces are in satisfactory agreement with the previous periodic slab DFT calculations.[5,6,11−13,29] The energy differences between associative and dissociative types of adsorption became less pronounced with the increasing number of adsorbed H_2O molecules. In the case of SnO_2 mixed (Figure 6c) and dissociative (Figure 8b) structures, the energy is practically the same.

In Table 4, we present the relaxations of oxide atoms in the top surface layers. As may be expected, the atomic displacements for the hydrated surfaces are much smaller (especially for the dissociative adsorption) than the case of the bare surfaces (Tables 2 and 4) due to saturation of the vacant coordination sites for the surface Sn up to the total coordination number 6. Analysis of the data of the Table 4 shows that shifts of a given metal atom (Me (V) or Me(VI)), as a rule, have an opposite sign for the associative and dissociative adsorption. For Sn atoms, vertical displacements are noticeably smaller than displacements of Ti atoms.

The positions of the H_2O O and terminal O atoms relative the Ti-level in unrelaxed slabs are also given in Table 4. The distinction between them is apparent for monolayer coverage by H_2O (i.e., the Ti(V)−O_{term} is shorter than the Ti(V)−OH_2)

TABLE 5: Distances between the Surface Metal and Oxygens Atoms (averaged results for five-Me-layer slabs and for $N_w = 2$ and $N_w = 8$ H_2O molecules on each side)

		distances, Å					
	[a]	assoc adsorption		mix. adsorption		dissoc adsorption	
crystal	atom pair	$N_w = 2$	$N_w = 8$	$N_w = 2$	$N_w = 8$	$N_w = 2$	$N_w = 8$
TiO_2	$Ti_{term}—O_{term}$			1.95	1.98	1.91	1.94[c]
	$Ti_V—O_{H2O}$	2.30	2.25 [b]	2.25	2.19		
	$Ti_{VI}—O_{br}$	1.88	1.89	1.88	1.89		
	$Ti_{VI}—O_{br(H)}$			2.04	1.99	2.02	2.00
SnO_2	$Sn_{term}—O_{term}$			2.09	2.10	2.05 (1.98)[d]	2.05— 2.07
	$Sn_V—O_{H2O}$	(2.19)[c]		2.21	2.18		
	$Sn_{VI}—O_{br}$	(2.00)		2.05	2.05		
	$Sn_{VI}—O_{br(H)}$			2.16	2.15	2.15 (2.08)	2.11

[a] See Table 4 f or designations of surface atoms. [b] Actual values lie in the interval 2.30—2.20 Å. [c] Actual values lie in the interval 1.88—2.00 Å. [d] LCAO B3LYP results[13] are given in parentheses.

but becomes insignificant after increasing the number of H_2O molecules. The difference in O positions is especially small in the cases of mixed adsorption with eight H_2O molecules.

In Table 5, we show the distances between the surface metal and O atoms calculated for mono- and two-layer adsorption. The second layer does not influence the Me—O bond lengths considerably, except for the distances between the Me(V) atom and H_2O O atom, which become shorter in the case of two-layer adsorption.

4. Conclusions

On the basis of the obtained results and within the models and assumptions on which our work is done, we can make the following conclusions:

1. The surface energy of SnO_2 (110) is noticeably larger than surface energy of TiO_2. We can suggest that there exists a correlation between the surface energy and water adsorption energy, ruling out the fact that cassiterite interacts more strongly with water than does rutile.

2. The basicity of O_{br} on the SnO_2 surface is greater than the basicity of O_{br} on the (110) TiO_2 surface because this atom type has an electronic energy state that is much higher than that of bulk cassiterite. The interaction of molecular H_2O with SnO_2 is accompanied by a larger redistribution of water electronic states than that of interaction with the TiO_2 surface.

3. Water adsorption on the (110) surface of TiO_2 is less energetically favorable than that of adsorption on the SnO_2 surface.

4. Monolayers of water prefer to be in molecular form on the TiO_2 (110) surface (considering the recent results,[10] up to 70% of water molecules are present in associated form). The fraction of the dissociated molecules on the SnO_2 surface is apparently larger.

5. The energy difference between associative, mixed, and dissociative types of adsorption becomes less pronounced with an increasing of number of adsorbed molecules because the surficial H-bonding network becomes less important with the availability of solvating H_2O molecules.

6. The vertical displacements of Sn atoms are noticeably smaller than displacements of Ti atoms on the hydroxylated surfaces.

7. In contrast to the TiO_2 case, both surface Sn atoms (Sn_{VI} and Sn_{term}) have the same vertical displacements in a mixed adsorption structure.

8. The second layer of H_2O molecules does not considerably influence on vertical displacements of surface Ti and Sn atoms, but it tends to decrease the distance between the O_{H2O} and Me(V) atoms.

9. Because of the nonvertical positions of O_{term} and O_{H2O} atoms above the Me(V), the difference between their z-coordinates is noticeably less than the difference between corresponding distances $Me_{term}—O_{term}$ and $Me_V—O_{H2O}$.

Acknowledgment. This research was supported by the U.S. Department of Energy, Office of Basic Energy Sciences, Division of Chemical Sciences, Geosciences and Biosciences, under the project "Nanoscale Complexity at the Oxide-Water Interface". A.V.B. thanks Russian Fund of Basic Research for support, grant 08-03-00438-a. Computation was supported by the Center for Environmental Kinetics Analysis (CEKA), an NSF Environmental Molecular Science Institute.

References and Notes

(1) Henderson, M. A. *Surf. Sci. Rep.* **2002**, *46*, 1.
(2) Cabailh, G.; Torrelles, X.; Lindsay, R.; Bikondoa, O.; Joumard, I.; Zegenhagen, J.; Thornton, G. *Phys. Rev. B* **2007**, *75*, 241403(R)
(3) Brinkley, T.; Dietrich, M.; Engel, T.; Farrall, P.; Gantner, G.; Schafer, A.; Szuchmacher, A. *Surf. Sci.* **1998**, *395*, 292.
(4) Goniakowski, J.; Gillan, M. J. *Surf. Sci.* **1996**, *350*, 145.
(5) Lindan, P. J. D.; Harrison, N. M.; Gillan, M. J. *Phys. Rev. Lett.* **1998**, *80*, 762.
(6) Zhang, C.; Lindan, P. J. D. *J. Chem. Phys.* **2003**, *118*, 8.
(7) Bates, S. P.; Kresse, G.; Gillan, M. J. *Surf. Sci.* **1998**, *409*, 336.
(8) Langel, W. *Surf. Sci.* **2002**, *496*, 141.
(9) Bandura, A. V.; Sykes, D. G.; Shapovalov, V.; Troung, T. N.; Kubicki, J. D.; Evarestov, R. A. *J. Phys. Chem. B* **2004**, *108*, 7844.
(10) Perron, H.; Vandenborre, J.; Domain, C.; Drot, R.; Roques, J.; Simoni, E.; Ehrhardt, J.-J.; Catalette, H. *Surf. Sci.* **2007**, *601*, 518.
(11) Lindan, P. J. D. *Chem. Phys. Lett.* **2000**, *328*, 325.
(12) Bates, S. P. *Surf. Sci.* **2002**, *512*, 29.
(13) Evarestov, R. A.; Bandura, A. V.; Proskurov, E. V. *Phys. Status Solidi B* **2006**, *243*, 1823.
(14) Becke, A. D. *J. Chem. Phys.* **1993**, *98*, 5648.
(15) Lee, C.; Yang, R. G.; Parr, R. G. *Phys. Rev. B* **1988**, *37*, 785.
(16) Sverjensky, D. A. *Geochim. Cosmochim. Acta* **2001**, *65*, 3643.
(17) Kresse, G.; Furthmüller, J. *Phys. Rev. B* **1996**, *54*, 11169.
(18) Kresse, G.; Furthmüller, J. *Vasp the Guide*; Institut für Material-physik, Universität Wien: Vienna, Austria, 2003.
(19) Perdew, J. P.; Burke, K.; Ernzerhof, M. *Phys. Rev. Lett.* **1996**, *77*, 3865.
(20) Perdew, J. P.; Wang, Y. *Phys. Rev. B* **1992**, *45*, 13244.
(21) Kresse, G.; Joubert, J. *Phys. Rev. B* **1999**, *59*, 1758.
(22) Blöchl, P. E. *Phys. Rev. B* **1994**, *50*, 17953.
(23) Monkhorst, H. J.; Pack, J. D. *Phys. Rev.* **1976**, *13*, 5188.
(24) Lindan, P. J. D.; Harrison, N. M; Gillan, M. J.; White, J. A. *Phys. Rev. B* **1997**, *55*, 15919.
(25) Hameeuw, K. J.; Cantele, G.; Ninno, D.; Trani, F.; Iadonisi, G. *J. Chem. Phys.* **2006**, *124*, 024708.
(26) Oviedo, J.; Gillan, M. J. *Surf. Sci.* **2000**, *463*, 93.
(27) Abraham, S. C.; Bernstein, J. L. *J. Chem. Phys.* **1971**, *55*, 3206.

(28) Bolzan, A. A.; Fong, C.; Kennedy, B. J.; Howard, C. J. *Acta Crystallogr., Sect. B: Struct. Crystallogr. Cryst. Chem.* **1997**, *53*, 373.
(29) Bandura, A. V.; Sofo, J. O.; Kubicki, J. D. *J. Phys. Chem. B* **2006**, *110*, 8386.
(30) Labat, F.; Baranek, Ph.; Adamo, C. *J. Chem. Theory Comput.* **2008**, *4*, 341.
(31) Perron, H.; Domain, C.; Roques, J.; Drot, R.; Simoni, E.; Catalette, H. *Theor. Chem. Acc.* **2007**, *117*, 565.
(32) Perdew, J. P.; Ernzerhof, M.; Burke, K. *J. Chem. Phys.* **1996**, *105*, 9982.
(33) Calatayud, M.; Markovits, A.; Menetrey, M.; Mguig, B.; Minot, C. *Catal. Today* **2003**, *85*, 125.
(34) Rosso, K. M.; Becker, U. *Geochim. Cosmochim. Acta* **2003**, *67*, 941.
(35) Mamontov, E.; Vlcek, L.; Wesolowski, D. J.; Cummings, P. T.; Wang, W.; Anovitz, L. M.; Rosenqvist, J.; Brown, C. M.; Sakai, V. G. *J. Phys. Chem. C* **2007**, *111*, 4328.

JP711763Y